# DETECTING THE DAMAGED AREAS CAUSED BY SINABUNG VOLCANO ERUPTION DURING 2013-2016 USING LANDSAT-8 MULTITEMPORAL

**Suwarsono, Hidayat, Totok Suprapto, Fajar Yulianto, Zylshal, Indah Prasasti, Parwati, M. Rokhis Khomarudin**
Remote Sensing Application Center, Indonesian National Institute of Aeronautics and Space (LAPAN)

suwarsono@lapan.go.id

**Abstract**. After inactive for centuries, in 2013 Sinabung Volcano active again with the enormity eruption that release a hot cloud, lava and pyroclastic flows. The eruption is said to have claimed lives and destroyed human settlements, agricultural land and existing infrastructure, particularly on the slopes of the south, southeast and east. During the period from 2013 to mid 2016, this volcano is still experiencing some major eruption, so it is possible having the affected area more extensively. This study aims to detect the damaged areas caused by the eruption in the period 2013 to 2016 by using a medium resolution satellite data, Landsat latest generation, the Landsat-8. The data used is a pair of multitemporal imagery, ie the first is recorded data before the eruption and second is data recorded during or after the eruption. The method is performed include the radiometric correction, land cover supervised classification, detection the areas affected by the eruption and GIS analysis to determine spatial-quantitatively the damages, namely in the context of the extents of each type of landcover that having damaged or destroyed by the eruption. The results showed that the medium resolution data Landsat-8 is very useful for use in detecting and mapping the damaged areas caused by the eruption of a volcano.

**Keywords**: Damaged areas, eruption, Sinabung Volcano, Landsat-8

## 1. Introduction

After inactive for centuries, in 2013 Sinabung Volcano active again with the enormity eruption that release a hot cloud, lava and pyroclastic flows. The eruption is said to have claimed lives and destroyed human settlements, agricultural land and existing infrastructure, particularly on the slopes of the south, southeast and east. Located in Karo Regency, North Sumatra Province (Kusumadinata 1979), Sinabung Volcano become the most active volcano in Sumatra since first catasthropic eruption in this century in November 2013. The volcano is classified as A-Type volcano by Centre for Volcanology and Geological Hazard Mitigation classifies Mount Sinabung into A-Type volcano (Sutawidjaja et al. 2013). Center for Volcanology and Geological Hazard Mitigation has reported that the potential hazard of the eruption of Mount Sinabung up to 11 September 2014 can be derived from: lava flows, incandescent lava and hot clouds that leads to the south and southeast as far as 5 kilometers. Also, there is the potential for secondary hazards from lahar that may occur due to high rainfall that is capable of transporting ash fall, tephra, lava debris, rock fragments through the river valleys (VSI ESDM 2014). Fig.1 showed ocation of the Sinabung Volcano in Sumatera.

The Landsat series of satellites has provided the long continuous data of the volcanoes activities in the world since 1972 (Suwarsonoet al. 2014). The Landsat TM has been used to calculate the total thermal flux for lava flowing in tubes, on the surface, or under shallow (Harriset al. 1998). By examining the composition of the short-wave infrared (SWIR) signal emitted from the flow surface, the Landsat ETM+ data can be used to understand the thermal characteristics of a series of lava flows

emplaced at the Mount Etna volcano, Sicily, during 27–28 October 1999 (Wrightet al. 2001). The geomorphic features can be delineated using the Landsat TM (Novakand Soulakellis 2000). The morphological changes in the drainage system and lahar detection also can be recognized using Landsat ETM+ (Davila et al. 2007). The Landsat TM also can be used to estimate the fractionalarea of the hottest part of an active flow and the temperature of the cooler crust of Mount Etna eruptions (Lombardo et al. 2004). Lava flows from 1938 up to the last eruption to date in 2010 can be mapped with Landsat-7 ETM+ (Benoîtet al. 2010). The Landsat-7 ETM+ also can be used to map the bifurcation and braiding of underground lava tubes and estimate effusion rates (Flynn et al. 2011) and Nyamulagira lava flows from 1938 up to the last eruption to date in 2010 (Flynn et al. 2011). Then, the affected areas of Sinabung Volcano eruption has tried to be detected using Landsat-8 based on reflectance change (Suwarsonoet al. 2014). The volume of pyroclastic deposits and morphological changes caused by the 2010–2015 eruption have been estimated using SPOT-6 DEM (Yulianto et al. 2016). The volume was approximately $2.8 \times 10^8$ $m^3$.

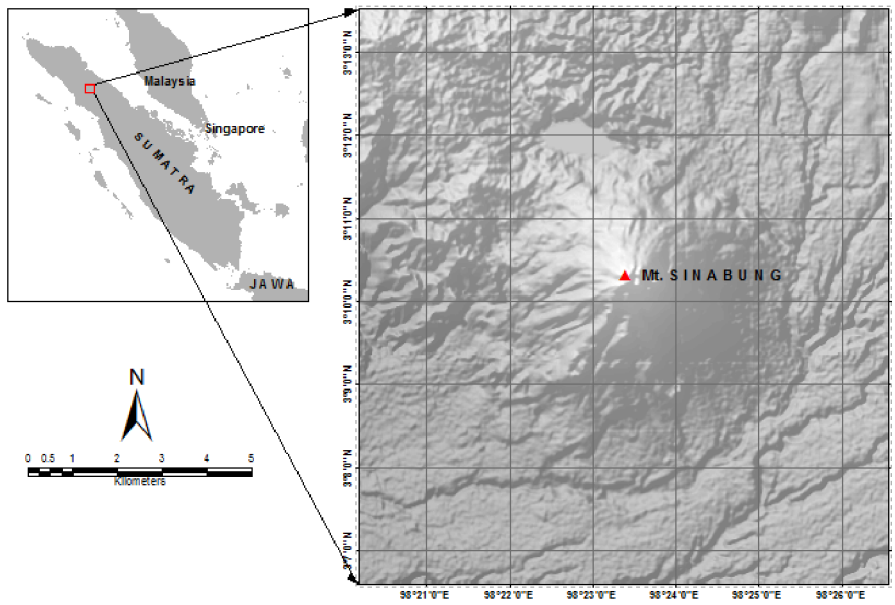


**Figure 1.** Location of the Sinabung Volcano in Sumatera.

During the period from 2013 to mid 2016, Sinabung Volcano is still experiencing some major eruption, so it is possible having the affected area more extensively. Regarding to disaster derived from this volcano and the opportunity use of Landsat-8 for volcano damage assessment, it is important to know the damages that has been caused by this eruption using the satellite. This study aims to detect the damaged areas caused by the eruption in the period 2013 to 2016 by using a medium resolution satellite data, Landsat latest generation, the Landsat-8.

## 2. Methods

The data used is a pair of multitemporal Landsat-8 imageries which cover Sinabung Volcano areas (path 129 row 058), i.e the first is recorded data before the eruption and second is data recorded during or after the eruption. The first image dated June 7, 2013 and the second image dated May30, 2016 (Fig.2). The first image shows the condition before the eruption of November 2013 and the second image shows the condition after recent eruption. In this research, Digital Elevation Model Shuttle Radar Topography Mission (DEM SRTM) 30 m resolution also used to correct the reflectance due to topograhic effects and to interpretation the topography.

The method is performed include the radiometric correction, land cover supervised classification, detection the areas affected by the eruption and GIS analysis to determine spatial-quantitatively the damages, namely in the context of the extents of each type of landcover that having damaged or destroyed by the eruption. The radiometric correction method consist of the digital number to reflectance convertion and the effect of topography correction. The USGS method is used to convert the digital number to reflectance (USGS 2015). C-correction method is used in topography effect correction. Detecting the areas affected by the eruption was done by thresholding methods based on reflectance change and NDVI resulted from the statistics calculation.

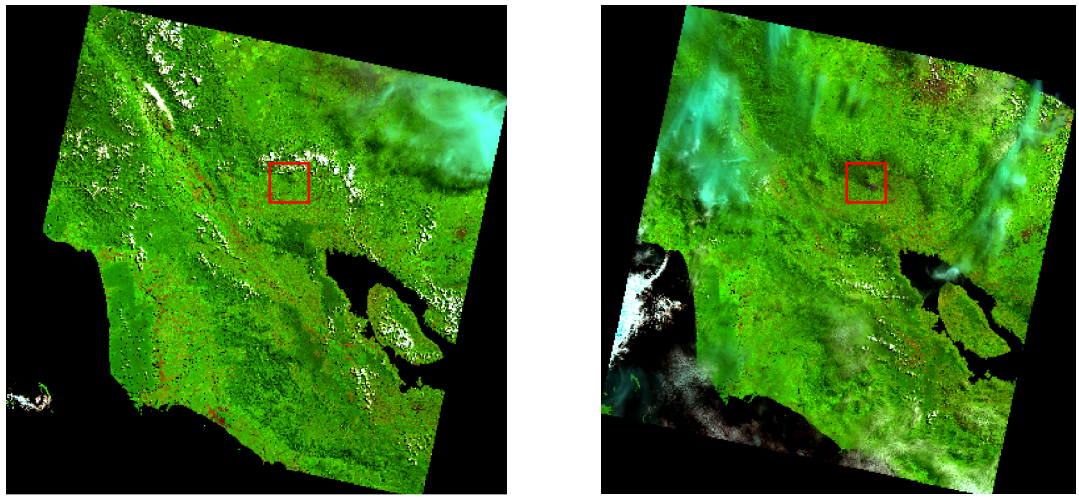

**Figure 2.** Landsat-8 coverage of path 128 row 059 date 7 June 2013 (left) and 30 May 2016 (right). Red box shows the Sinabung Volcano location.

*2.1. Digital number to reflectance convertion*

The following equation is used to convert DN values to TOA reflectance for OLI[13]:

$$\rho\lambda' = M\rho Qcal + A\rho \quad \text{.....(1)}$$

where $\rho\lambda'$ is TOA planetary reflectance (without correction for solar angle). $M\rho$ is Band-specific multiplicative rescaling factor from the metadata (REFLECTANCE_MULT_BAND_x, where x is the band number), $A\rho$ is band-specific additive rescaling factor from the metadata (REFLECTANCE_ADD_BAND_x, where x is the band number), and Qcal is quantized and calibrated standard product pixel values (DN).

Then, sun angle correction of TOA reflectance can be calculated by using the following equation(USGS 2015):

$$\rho\lambda = \frac{\rho\lambda'}{\cos(\theta sz)} = \frac{\rho\lambda'}{\sin(\theta se)} \quad \text{.....(2)}$$

Where $\rho\lambda$ is TOA planetary reflectance, $\theta se$ is local sun elevation angle. The scene center sun elevation angle in degrees is provided in the metadata (SUN_ELEVATION). $\theta sz$ is local solar zenith angle, $\theta sz = 90° - \theta se$.

*2.2. Effect of Topography correction*

To reduce the topographic influence of Landsat 8 images which cover Sinabung Volcano region, C-correction method was implemented. This method is semi-empirical approach (Teilletet al. 1982).

This method were implemented for Landsat data processing in operational of the project of INCAS (Indonesian National Carbon Accounting) (Trisakti et al. 2009). The equation for calculating the corrected reflectance using the c-correction methods as follow:

$$LH = LT \times \frac{\cos z + c}{\cos i + c} \quad \text{.....(3)}$$

Where LH is reflectance of a horizontal surface, LT is reflectance of an inclined surface, z is solar zenith angle, i is local solar incident angle, c = b/m for LT = m × cos i + b. m is gradient of regression line: LT – cos i, and b is intercept of line: LT – cos i. Cos i is the solar illumination angle between solar incident angle and local surface normal. Cos i varies from -1 (minimum) to +1 (maximum), which can be calculated as follows:

$$\cos i = \cos e \cos z + \sin e \sin z \cos (a-a') \quad \text{.....(4)}$$

Where i is local solar incident angle, e is slope angle, z is solar zenith angle, a is solar azimuth angle, and a' is aspect angle. Solar zenith angle and solar azimuth angle were provided in Landsat-8 metadata file (MTL), whereas slope angle and aspect angle can be derived from DEM SRTM.

We use the c-factor for c-correction of topographic effect from the previous research result. The values of factor c for each band of Landsat-8 is shown on Table 1.

**Table 1**. The values of factor c for each band of Landsat-8 (Suwarsono et al. 2014)

| Band | b | m | c |
|---|---|---|---|
| **1** | 0.083 | 0.001 | 63.923 |
| **2** | 0.063 | 0.002 | 39.438 |
| **3** | 0.047 | 0.004 | 11.850 |
| **4** | 0.029 | 0.003 | 10.556 |
| **5** | 0.190 | 0.040 | 4.708 |
| **6** | 0.078 | 0.017 | 4.565 |
| **7** | 0.029 | 0.006 | 4.742 |
| **8** | 0.039 | 0.003 | 12.516 |
| **9** | 0.001 | 0.000 | 30.000 |

## 3. Results and discussion

The data used is a pair of multitemporal Landsat-8 imageries which cover Sinabung Volcano areas (path 129 row 058), ie the first is recorded data before the eruption and second is data recorded during or after the eruption. The first image dated June 7, 2013 and the second image dated May 30, 2016. The first image shows the condition before the eruption of November 2013 and the second image shows the condition after recent eruption in May 2016. In this research, Digital Elevation Model Shuttle Radar Topography Mission (DEM SRTM) 30 m resolution also used to interprete the topography condition and to correct the reflectance due to topograhic effects.

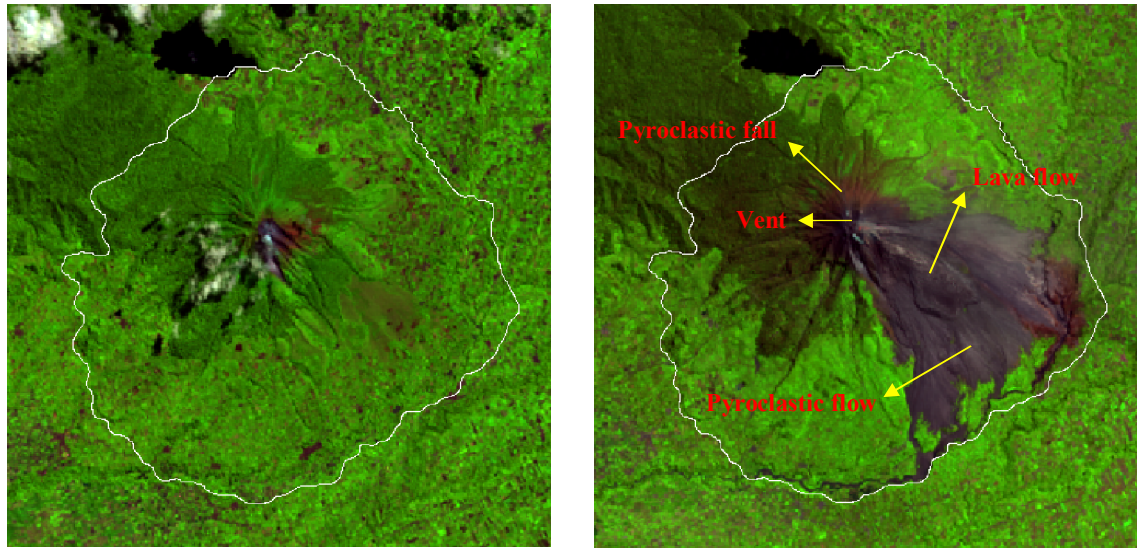


**Figure 3.** The stratovolcanic region of Sinabung Volcano (white color) date 7 June 2013 (left) and 30 May 2016 (right). Modified from Suwarsono et al. (2014)

Landsat-8 date 30 May 2016 show recent spreading of the affected area due to Sinabung Volcano eruption. From the composite band RGB 654, there can be identified three major deposition product from Sinabung Volcano eruption, ie lava, pyroclastic flow and pyroclastic fall. Lava flow show the purple color and look massive shape. Pyroclastic flow show the light purple and look flowing shape. Both have southern, southern east and eastern direction. Pyroclastic fall show the brown and reddish color.

The results showed that the broad interpretation of the geomorphology of the area planimetric volcanic Sinabung Volcano, a modification of a previous study (Suwarsono et al. 2014), is about 4,695 ha (Fig.3). The results of the previous interpretation provides comprehensive results of 4,251 ha (Suwarsono et al. 2014). So there is the addition of an area of approximately 444 ha. This is because the results of this latest interpretation of the data using Landsat-8 later that has described the current condition updates. That is the latest interpretation of this result considering the effects of the eruption in May 2016 was wider than what was previously thought. In the previous interpretation using Landsat-8 dated March 22, 2014, whereas this recent study using images dated May 30, 2016.

Several training areas took in both derived reflectance corrected images. Then we measured the statictics of reflectance values from visible, Near Infra Red, and Short Wave Infra Red bands. There were identified to several types of changes, from vegetated areas(forest, shrubland, cropland) to damaged areas or areas that were covered by eruption products (lava or pyroclastic). Fig 4 showed Landsat-8 OLI spectral response to surface cover change types due to the eruption of Sinabung Volcano 2013-2016. Based on the graph, generally there can be understood that the reflectance of band 5 has the highest values for forests, shrublands, barelands, and also settlements. But for cropland, band 6 has more reflectance values than others. Also, generally, Band 5 has the highest values for volcanic eruption product of lava and pyroclastic flow. But for pyroclastic fall, band 6 has the highest values. Table 2 show the changes of reflectance values from all surface covers to volcanic eruption deposits.

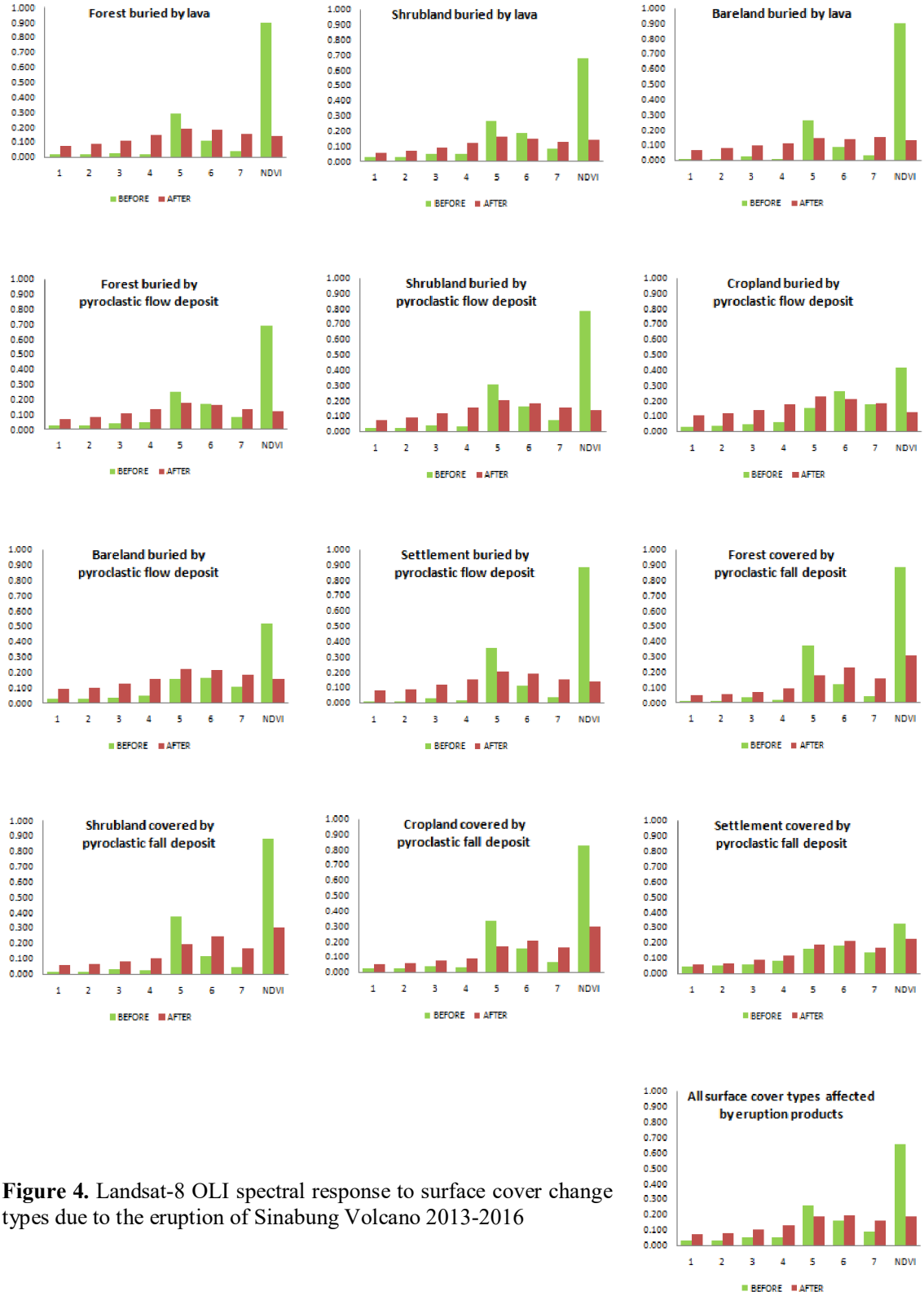


**Figure 4.** Landsat-8 OLI spectral response to surface cover change types due to the eruption of Sinabung Volcano 2013-2016

**Table 2**. The changes of reflectance values from all surface covers to volcanic eruption deposits

| **Before eruption** | | | | | | | | |
|---|---|---|---|---|---|---|---|---|
| | 1 | 2 | 3 | 4 | 5 | 6 | 7 | NDVI |
| **Mean** | 0.030 | 0.033 | 0.048 | 0.051 | 0.261 | 0.157 | 0.084 | 0.658 |
| **Sdev** | 0.004 | 0.004 | 0.005 | 0.007 | 0.029 | 0.013 | 0.010 | 0.045 |
| **After eruption** | | | | | | | | |
| | 1 | 2 | 3 | 4 | 5 | 6 | 7 | NDVI |
| **Mean** | 0.071 | 0.081 | 0.102 | 0.131 | 0.190 | 0.195 | 0.158 | 0.188 |
| **Sdev** | 0.008 | 0.009 | 0.011 | 0.013 | 0.018 | 0.018 | 0.019 | 0.018 |
| **Changes** | | | | | | | | |
| | 1 | 2 | 3 | 4 | 5 | 6 | 7 | NDVI |
| **Mean** | -0.041 | -0.048 | -0.054 | -0.080 | 0.071 | -0.038 | -0.038 | -0.470 |
| **Sdev** | 0.009 | 0.010 | 0.011 | 0.014 | 0.036 | 0.021 | 0.021 | -0.048 |

NDVI value were also calculated (Suwarsono et al. 2014).The NDVI values derived from Landsat-8 were calculated by using the following aquation (Suwarsono et al. 2014):

$$\text{NDVI} = \frac{\rho 5 - \rho 4}{\rho 5 + \rho 4} \quad \text{.....(5)}$$

Where ρ4 and ρ5 are reflectance values of band 4 and 5 respectively. Also, normalized distance (D values) were calculated to measure and to test the discrimination ability of the index. The D-values > 1 will represent good separability of the index to discriminate the volcanic deposits and nonnvolcanic deposits. Below is the equation for calculating D-values (Kaufman and Remer 1994):

$$\text{D} = \left|\frac{\mu 2 - \mu 1}{\sigma 2 + \sigma 1}\right| \quad \text{.....(6)}$$

Where D is Normalized Distance, μ1 and μ2 are mean values of samples before and after eruption respectively, σ1 and σ2 are deviation standard of samples before and after eruption respectively. The results calculation of the D-value for all bands and NDVI as shown below (Table 3).

**Table 3**. D-value of spectral bands and NDVI of Landsat-8 OLI

| **Origin** | **Current** | 1 | 2 | 3 | 4 | 5 | 6 | 7 | NDVI |
|---|---|---|---|---|---|---|---|---|---|
| **Forest** | Lava deposit | 1.64 | 1.18 | 1.68 | 0.77 | 12.89 | 4.31 | 1.72 | 80.87 |
| **Shrubland** | Lava deposit | 3.44 | 3.20 | 4.10 | 3.42 | 14.77 | 10.60 | 5.92 | 92.39 |
| **Bareland** | Lava deposit | 4.48 | 5.48 | 7.03 | 8.24 | 7.68 | 8.39 | 1.89 | 4.85 |
| **Forest** | Pyroclastic Flow deposit | 5.40 | 4.48 | 6.58 | 3.09 | 46.97 | 20.12 | 8.78 | 150.44 |
| **Shrubland** | Pyroclastic Flow deposit | 5.96 | 5.13 | 6.39 | 4.75 | 24.83 | 18.42 | 11.06 | 80.35 |
| **Cropland** | Pyroclastic Flow deposit | 1.18 | 1.08 | 1.60 | 1.12 | 6.90 | 3.69 | 1.92 | 39.02 |
| **Bareland** | Pyroclastic Flow deposit | 4.02 | 3.89 | 3.34 | 3.02 | 5.48 | 7.90 | 5.88 | 24.90 |
| **Settlement** | Pyroclastic Flow deposit | 2.73 | 2.54 | 3.15 | 4.15 | 13.80 | 10.86 | 7.07 | 31.42 |
| **Forest** | Pyroclastic Fall deposit | 3.58 | 3.08 | 7.35 | 3.56 | 35.02 | 6.32 | 3.29 | 72.07 |
| **Shrubland** | Pyroclastic Fall | 3.65 | 3.39 | 5.93 | 3.28 | 48.27 | 9.91 | 4.54 | 58.87 |

| | | | | | | | | | |
|---|---|---|---|---|---|---|---|---|---|
| | deposit | | | | | | | | |
| **Cropland** | Pyroclastic Fall deposit | 3.82 | 3.49 | 5.13 | 3.04 | 14.31 | 9.22 | 4.36 | 22.26 |
| **Settlement** | Pyroclastic Fall deposit | 8.15 | 7.40 | 10.42 | 8.52 | 12.11 | 25.73 | 13.11 | 5.76 |
| **Average** | | 4.00 | 3.69 | 5.22 | 3.91 | 20.25 | 11.29 | 5.80 | 55.27 |

The variables of ρ1, ρ2, ρ3, ρ4, ρ5, ρ6, ρ7, and NDVI showed the D-value>1, therefore they have good separabilty to discriminate the volcanic deposits and non volcanic deposits. Compared with the results of previous research (Suwarsono et al. 2014), thus demonstrating that the results of the analysis of the latest data on the results of this study provide the D-value is higher. In other words, this result is able to uncover the ability of each band in a separate area affected and not affected by the eruption.One other important thing is that this result also showed that NDVI parameter has is the highest of D-value compared with the another parameters of single band.Fig. 5 showed visually the change detection using Landsat-8 OLI RGB every single band OLI and NDVI. Therefore, NDVI variables were done as the threshold. The threshold based on mean (μ) and deviation standard (σ) values (Table 5). Based on the normal distribution asumption, be chosen the values of μ ± 2 σ as the threshold values for affected areas discrimination. Then, damaged areas pixels are extracted by applying the thresholds of $NDVI_{post}$ and dNDVI. The pixel defined as damaged areas if meet the following criterias:

$$DA_{ij} = \begin{matrix} dNDVI_{ij} \leq -0.465 \\ NDVIpost_{ij} \leq 0.224 \end{matrix} \quad \text{..... (7)}$$

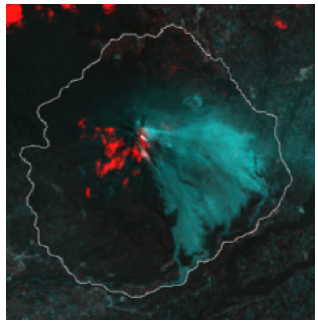
Band 1

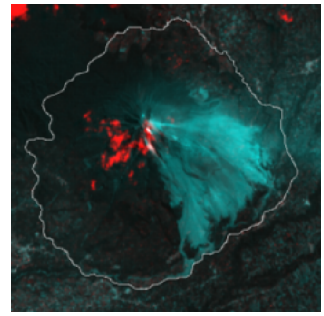
Band 2

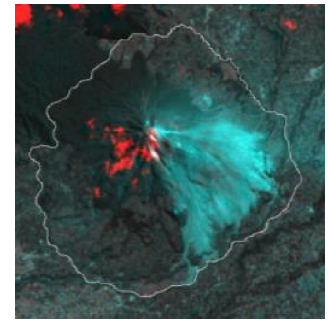
Band 3

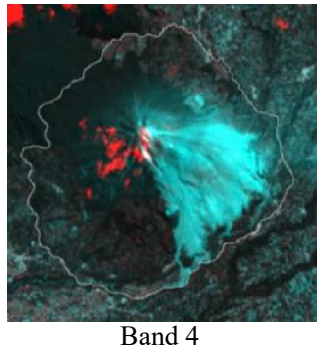
Band 4

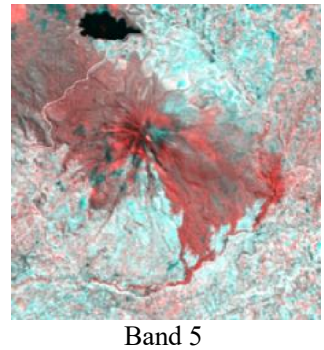
Band 5

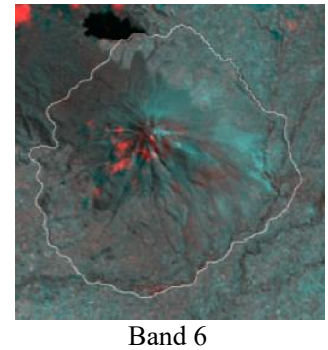
Band 6

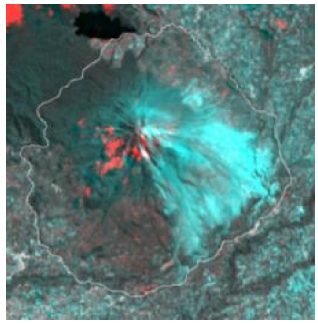

Band 7

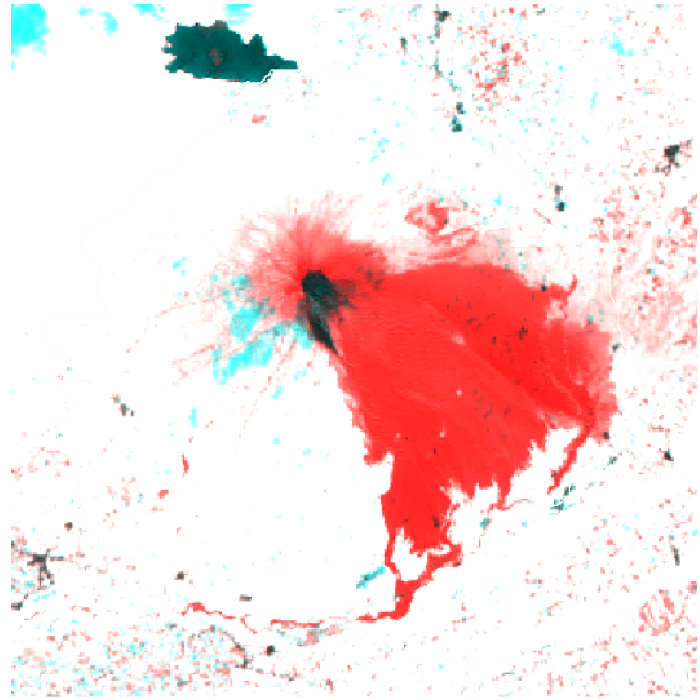

NDVI

**Figure 5.** The change detection using Landsat-8 OLI RGB every single band OLI and NDVI. Red color indicates the damaged areas.

Whereas DAij is damaged area pixels, $dNDVI_{ij}$= $NDVIpost_{ij}$- $NDVIpre_{ij}$. $NDVIpre_{ij}$ is NDVI values of images before eruption for pixel ij and $NDVIpost_{ij}$ is NDVI values of images after eruption for pixel ij. The result of implementation of this formula can be seen in Fig.6.

When the results were compared with the appearance of the Landsat-8 RGB color composite image 654 (Fig. 6), then visually can be seen that the results of parameter estimation using NDVI already provides a good overview of the results.Although it still leaves some small part locations in the image off of detection,especially in some small parts of the affected pyroclastic fall near the crater.

Despite having several small parts locations in the image off of detection. Especially in some parts of the affected small pyroclastic fall near the crater.

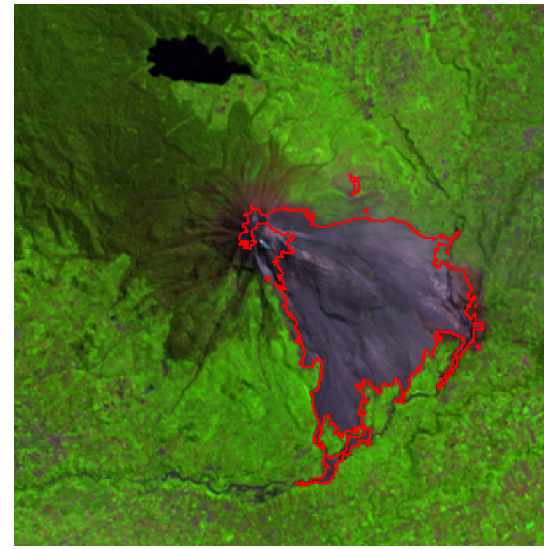

**Figure 6.** The result of the estimation of damaged areas based on NDVI parameter (Formula 7), red color lines, compiled with Landsat-8 RGB 654 date on 30 May 2016 (image of after eruption).

The results showed that the direction of the distribution of the products eruptions, lava and pyroclastic flows mainly relatively very broad and likely to lead to the east and southeast. The result also showed that approximately 995.7 ha (21.2 % of the Sinabung Volcanic region) were damaged.

**Table 4**. Assessment of the damaged areas due to Sinabung Volcano eruption during 2013-2016

| No | Type | Squares (Ha) | Damaged Areas (Ha) | % Damaged |
|---|---|---|---|---|
| 1 | Cropland | 2,622.2 | 598.9 | 22.8 |
| 2 | Shrubland | 607.5 | 255.4 | 42.0 |
| 3 | Forest | 1,358.4 | 136.8 | 10.1 |
| 4 | Bareland | 71.8 | 0.0 | 0.0 |
| 5 | Settlement | 34.6 | 4.7 | 13.5 |
| 6 | Water | 0.2 | 0 | 0.0 |
| | sum | 4,694.6 | 995.7 | |

Then, land cover classification results showed that land cover in the Sinabung Volcano region is dominated by cropland (2,622.2 ha), forest (1,358.4 ha) and shrubland (607.5 ha). In addition, important to note that the region found many locations settlement with an area of approximately 34.6 hectares settlements.During the 2013-2016 eruptions range, based on the results of detection, approximately 995.7 ha of the area were damaged, those are cropland (598.9 ha), shrubland (255.4 ha), forest (136.8 ha), and housing (4.7 ha). Table 4 shows sssessment of the damaged areas due to Sinabung eruption during 2013-2016. Spatially, can be seen also in Fig.7.

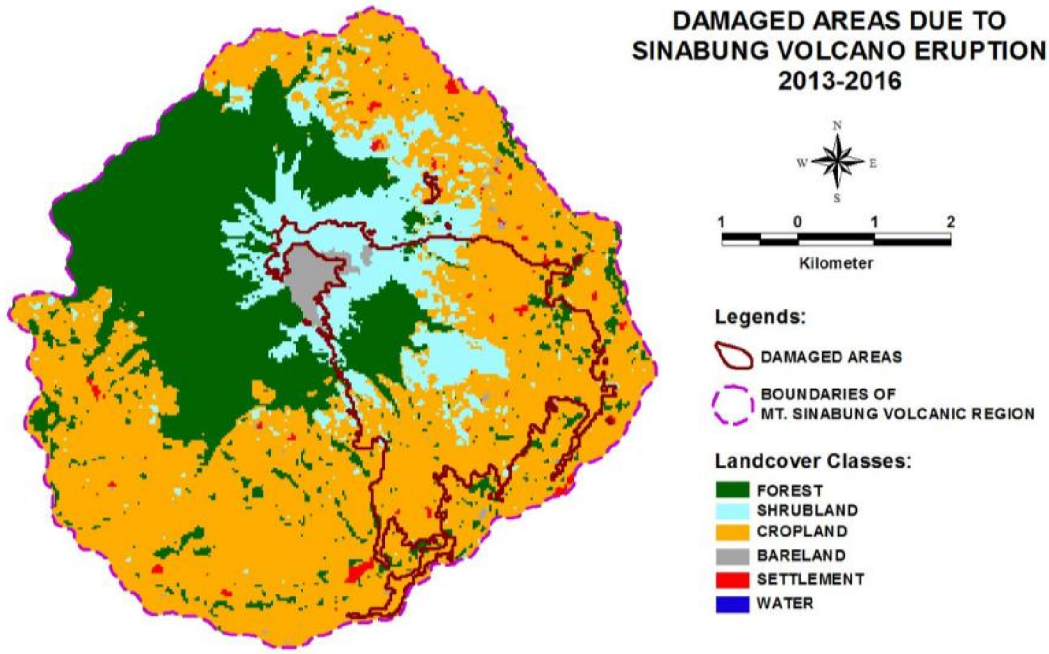


**Figure 7.** The landcover of Sinabung Volcano region and boundaries of the damaged areas due to the eruption during 2013-2016.

We have conducted the field observation in 2015. Some of the informations gain from the activity was used to verify the results of analysis. Fig. 8 showed the field conditions the affected areas due to Sinabung eruption. We got pictures of lava and pyroclastic flow, the settlements affected by pyroclastic fall, citrus plantations affected by pyroclastic fall, and also the pyroclastic flow entering the river channel. All the informations (damaged areas) matched closely with the the results of analysis.

**4. Conclusion**

Landsat-8 is very useful for use in detecting and mapping the damaged areas caused by the eruption of a volcano.NDVI is more sensitive rather than single band for the detection of all cover types among forest, shrubland, cropland, bareland and also for settlement on the volcanic region. At least, the extent of damaged area due to Sinabung Volcano eruption during 2013-2016 is estimated nearly a thousand ha or about fifth of the Mt. volcanic region. Most of them is vegetated areas such forest, shrubland, and cropland.The analysis for another cases of volcanoes in Indonesia is needed to give the better and more comprehensive results, in the context of the use of Landsat 8 for observation of the effects of volcanic eruptions in Indonesia.

The crater of Sinabung during eruption

Pyroclastic flow entering the river channel

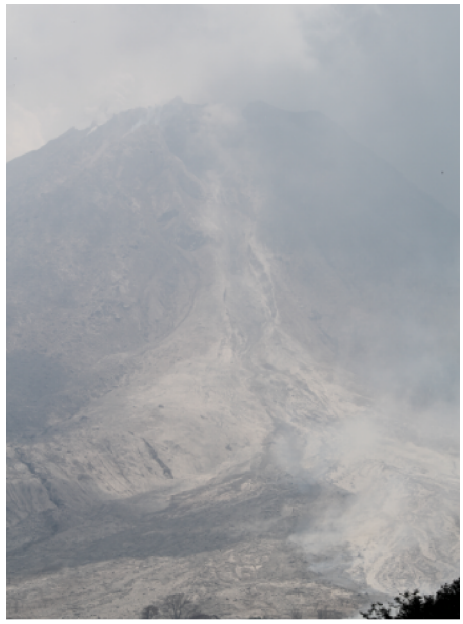

Lava and pyroclastic flow

Citrus plantations affected
by pyroclastic fall

Settlements affected by pyroclastic fall

Settlements affected by pyroclastic fall

**Figure 8.** Field conditions the affected areas due to Sinabung eruption

**Acknowledgement**
Thanks to Director of Remote Sensing Technology and Data Center of LAPAN and staffs who have provided the Landsat-8. Thanks also to Mr. Taufik Maulana dan Dr. Wikanti Asriningrum for the discussion, advices and suggestions in this research.

**References**

Benoît, S.B., W. Christelle and N. d'Oreye 2010 A new map of the lava flow field of Nyamulagira (D.R. Congo) from satellite imagery *Journal of African Earth Science***58**: 778-786.

Davila, N., L. Capra, J.C. Gavilanes-Ruiz, N. Varley, G. Norini and A.G. Vazquez 2007 Recent lahars at Volcán de Colima (Mexico): Drainage variation and spectral classification *Journal of Volcanology and Geothermal Research***165**: 127-141.

Flynn, L.P., A.J.L. Harris, R. Wright 2001 Improved identification of volcanic features using Landsat 7 ETM+*Remote Sensing of Environment***78**: 180-193.

Harris, A.J.L., Flynn, L.P., Keszthelyi, L., Mouginis-Mark, P.J., Rowland, S.K., Resing, J.A 1998 Calculation of lava effusion rates from Landsat TM data*Bulletin of Volcanology***60**: 52-71.

Kaufman, Y.J. and L.A. Remer 1994Detection of forest fire using Mid-IR reflectance: and application fro aerosols study *IEEE Transactions on Geoscience and Remote Sensing***32**,672-683.

Kusumadinata, K 1979*Data dasar gunung api indonesia* (Direktorat Vulkanologi, Bandung)

Lombardo, V., M.F. Buongiorno, D.Pieri and L. Merucci 2004 Differences in Landsat TM derived lava flow thermal structures during summit and flank eruption at Mount Etna*Journal of Volcanology and Geothermal Research***134**: 15-34.

Novak, I.D. and N. Soulakellis 2000 Identifying geomorphic features using LANDSAT-5 TM data processing techniques on Lesvos, Greece*Geomorphology***34**: 101-109.

Sutawidjaja, I.S., O. Prambada, D.A. Siregar 2013 The August phreatic eruption of Mount Sinabung, North Sumatra*Indonesian Journal of Geology***8** (1): 55-61.

Suwarsono, Hidayat, J.T. Nugroho, Wiweka, Parwati and M. Khomarudin 2014 Detecting the affected areas of Mount Sinabung eruption using Landsat-8 based on reflectance change*Proceeding PORSEC 2014*

Teillet, P., B.Guindon, and D. Goodenough 1982 On the slope-aspect correction of Multispectral Scanner Data*Canadian Journal of Remote Sensing***8**(2): 84-106.

Trisakti, B., M.Kartasasmita, Kustiyo, T. Kartika 2009 Kajian koreksi terrain pada citra Landsat Thematic Mapper (TM)*Jurnal Penginderaan Jauh dan Pengolahan Data Citra Digital***6**, 1-10.

USGS 2015*Landsat 8 (L8) Data Users Handbook Version 1.0*. (EROS Sioux Falls, South Dakota)

VSI ESDM Http://www.vsi.esdm.go.id/index.php/gunungapi/aktivitas-gunungapi/622-evaluasi-tingkat-aktivitas-siaga-level-iii-g-sinabung-hingga-tanggal-11-september-2014. Accessed on Oktober 18, 2014.

Wright, R., L.P. Flynn, and A.J.L. Harris 2001 Evolution of lava flow-field at Mount Etna, 27-28 October 1999, observed by Landsat 7 ETM+ *Bulletin of Volcanology***63**: 1-7

Yulianto, F., Suwarsono, P. Sofan 2016 The Utilization of Remotely Sensed Data to Analyze the Estimated Volume of Pyroclastic Deposits and Morphological Changes Caused by the 2010–2015 Eruption of Sinabung Volcano, North Sumatra, Indonesia*Pure Appl. Geophys.***173**(8): 2711-2725, doi:10.1007/s00024-016-1342-8.